*The definitive version was published in Science, **2023**, 380, 1043-1048, DOI: 10.1126/science.adg2833.*

https://science.org/doi/10.1126/science.adg2833

Synthesis and isolation of a triplet bismuthinidene with a quenched magnetic response

Authors: Yue Pang,[1] Nils Nöthling,[1] Markus Leutzsch,[1] Liqun Kang,[2] Eckhard Bill,[2] Maurice van Gastel,[1] Edward Reijerse,[2] Richard Goddard,[1] Lucas Wagner,[1] Daniel SantaLucia,[1] Serena DeBeer,[2] Frank Neese,[1]* Josep Cornella[1]*

Affiliations: [1]Max-Planck-Institut für Kohlenforschung, Kaiser-Wilhelm-Platz 1, 45470, Mülheim an der Ruhr, Germany.

[2]Max Planck Institute for Chemical Energy Conversion, Stiftstrasse 34-36, 45470, Mülheim an der Ruhr, Germany

*Correspondence to: neese@kofo.mpg.de; cornella@kofo.mpg.de;

Abstract: Large spin-orbit coupling (SOC) is an intrinsic property of the heavy elements that directly affects the electronic structures of the compounds. Herein we report the synthesis and characterization of a mono-coordinate bismuthinidene featuring a rigid and bulky ligand. All magnetic measurements [superconducting quantum interference device (SQUID), nuclear magnetic resonance (NMR)] point to a diamagnetic compound. However, multiconfigurational quantum chemical calculations predict the ground state of the compound to be dominated by a spin-triplet. The apparent diamagnetism is explained by an extremely large SOC-included positive zero-field splitting of more than 4500 wavenumbers, thus leaving a $M_S = 0$ magnetic sublevel thermally isolated in the electronic ground state.

One Sentence Summary: A stable and isolable mono-coordinate bismuthinidene complex features a unique "non-magnetic" triplet ground state as a result of its intrinsic relativistic properties.

Main Text: Molecular compounds with unpaired electrons typically manifest paramagnetism and anhanced reactivity (*1*, *2*). Transition metals and lanthanides are the prototypical examples of elements that form stable and isolable compounds while accommodating multiple unpaired electrons in their frontier *d*- and *f*-orbitals (*3*). In the realm of transition metals, countless examples of complexes supporting between 1-5 unpaired electrons at the metal site are well known (Fig. 1A, top). In the lanthanide series, more than five unpaired electrons can be accommodated, as highlighted by the six unpaired electrons in the *f*-orbitals in the lanthanide shift reagent $Eu(dpm)_3$ (dpm = dipivalomethonate) and the seven unpaired electrons in the *f*-orbitals of the MRI contrast agent Gd-DO3A-butrol (Gadobutrol). Whereas isolation and characterization of such compounds has become routine and textbook knowledge for transition metals, stark differences exist for *p*-block-based analogs (Fig. 1A, bottom). Indeed, the discovery of Gomberg's dimer (which equilibrates with the persistent

triphenylmethyl radical) (*4*, *5*), opened the door to the development and isolation of a plethora of persistent or stable radicals with one unpaired electron in the *p*-shell (*6*, *7*). Whereas, multi-centered diradical species—two unpaired electrons—based on *p*-block elements are well-known (e.g. O_2 molecule) (*8*), stable and isolable *single-centered diradicals* still remain elusive. Triplet carbenes, nitrenes and pnictinidenes are examples of such species, and the long-term quest for their isolation still remains a challenge (*9*–*11*). Initial efforts by Tomioka demonstrated the existence of a persistent triplet carbene in solution, albeit its high reactivity prevented isolation (*12*, *13*). To date, only two stable nitrene and phosphinidene compounds have been reported and described featuring closed-shell ground states (Fig. 1B, *14*, *15*). Recently, a metallonitrene was reported by Schneider and Holthausen, with two parallel-spin unpaired electrons mostly centered at the nitrene nitrogen atom (*16*); the high reactivity of the compound prevented its isolation. Therefore, it was structurally characterized *in-situ* by X-ray diffraction analysis as well as in solution at low temperatures. Collectively, these precedents clearly suggest that the synthesis and isolation of a single-centered stable diradical compound based on a main group element are , together, an enormous challenge which, if realized, would open the door to the study of unexplored electronic states of matter. Hence, within our interest in low-valent Bi compounds (*17*), we speculated that bismuthinidenes could serve as an ideal platform to isolate a single-centered *p*-block diradical. Herein, we present a bismuthinidene that features a single C–Bi(I) bond, flanked by rigid, non-coordinating and bulky "wings" that prevent the Bi(I) center from decomposition or dimerization. The compound features remarkable thermal stability both in solution and in the solid state, and can be isolated and stored in gram-quantities. A range of advanced spectroscopic measurements, combined with an in-depth computational analysis, permitted a complete understanding of its unusual electronic structure.

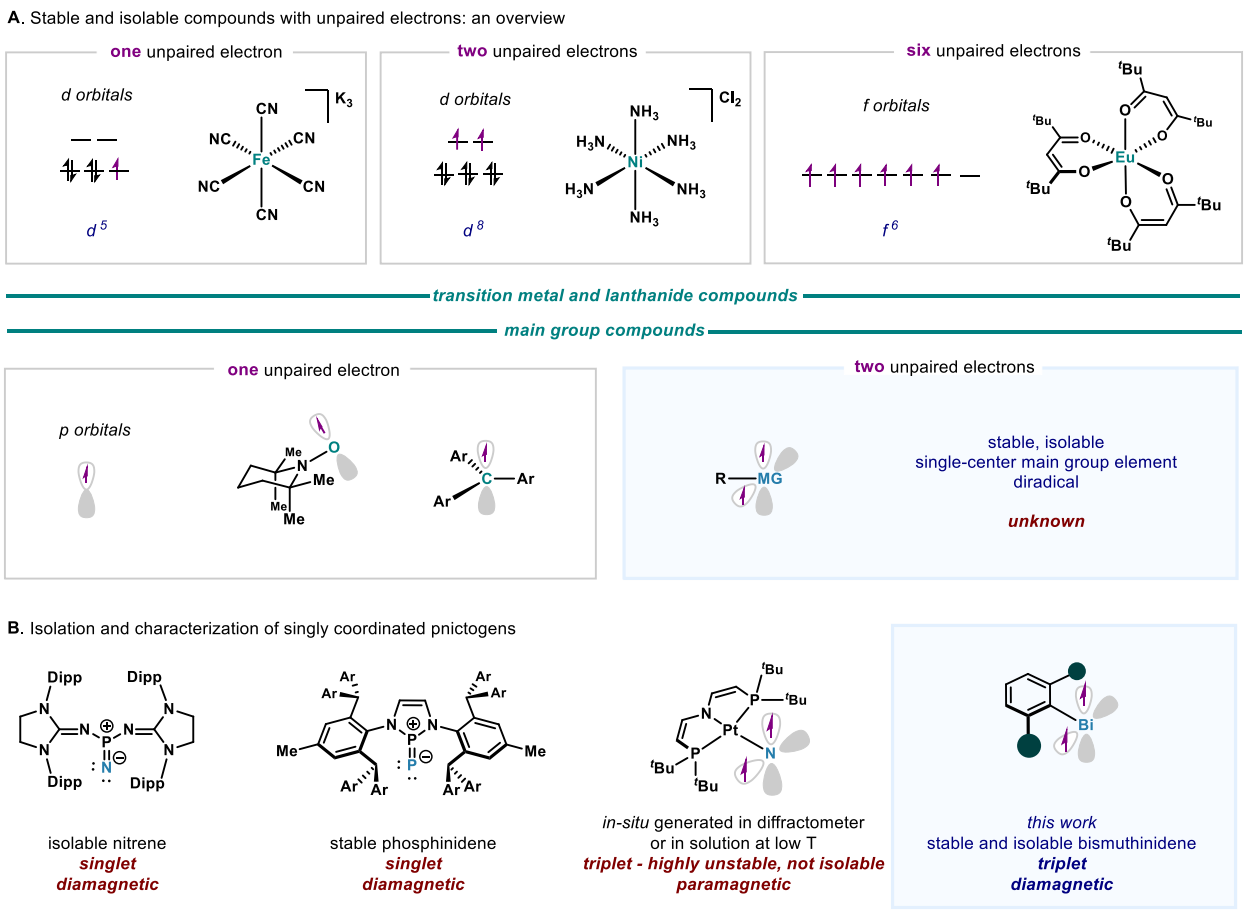

Fig. 1. A. Examples of stable and isolable transition metal, lanthanide and main group compounds bearing unpaired electrons in the frontier orbitals. B. State-of-the-art examples of singly coordinated nitrenes and pnictinidenes.

Triplet ground states of Bi(I) species were suggested for the gas phase for BiH and BiMe species (*18*–*20*). Yet, in the condensed phase, Bi(I) compounds have a strong tendency to dimerize to form dibismuthenes or oligomerize (*21*–*23*). However, the presence of additional Lewis-base donors permits isolation of monomeric Bi(I) compounds in the singlet form, such as Dostal's *N*,*C*,*N*-pincer bismuthinidenes (*24*–*26*). Inspired by the work of Matsuo and Tamao (*27*), we reasoned that the rigid, non-coordinating and bulky ^{t}Bu-M^{s}Fluind ligand could serve as a platform to stabilize the monomeric mono-coordinate Bi(I). Along these lines, we successfully synthesized the precursor ^{t}Bu-M^{s}Fluind-BiBr$_2$ (**1**) from the parent aryl bromide (**S3**). When **1** was reduced with 2.0 equivalents of cobaltocene in toluene under argon atmosphere at 25 °C, ^{t}Bu-M^{s}Fluind-Bi(I) (**2**) was obtained in 81% yield on a gram scale (Fig. 2A). Whereas all reported Bi(I) compounds thus far have an intense deep-blue/green color (*21*–*26*), **2** is bright yellow, suggesting a distinctive electronic structure. A single crystal X-ray structure analysis unequivocally revealed that **2** is a mono-coordinate bismuthinidene (Fig. 2B). Whereas a Bi(I) analogue without ^{t}Bu groups in the flanking wings ([M^{s}Fluind-Bi(I)]$_2$, **S2**) possesses a typical Bi=Bi bond of 2.8464(4) Å (see Supplementary Materials), the shortest Bi···Bi distance (4.385 Å) in the monomeric structure of **2** is larger than the sum of Bi···Bi van der Waals radii of 4.14 Å (*28*). Additionally, no solvent molecule is intercalated between the ligand scaffold and in the vicinity of the metal center. The

Bi−C(sp^2) bond distance in **2** clearly suggests a single bond [Bi1−C1: 2.2783(10) Å; cf. 2.26 Å (*29*)], which differs from the reported *N*,*C*,*N*-pincer bismuthinidenes, where the Bi−C(sp^2) bond distances indicate partial double bond character [from 2.138(10) Å to 2.222(5) Å (*24*, *25*, *30*–*32*)]. The absence of Bi−H bonds was confirmed by IR and ^{1}H NMR, combined with reactivity studies (*vide infra*). In sharp contrast to **1**, the Bi center is centrally situated (C4−C1−Bi1, for **1**: 163.27°; for **2**: 178.78°). The distances between the Bi center and the 9-fluorenyl arms (C9, C14 and their identical atoms; 3.427 to 3.870 Å) lie at the edge of the sum of Bi···C van der Waals radii of 3.77 Å (*28*, *33*), indicating a negligible Bi···ligand interaction. As suggested by NMR, **2** is symmetric and non-dynamic in solution, in the range of –70 to 90 °C, in line with the solid-state structure; diffusion-ordered NMR spectroscopy (DOSY) further supports the monomeric form of **2** in solution.

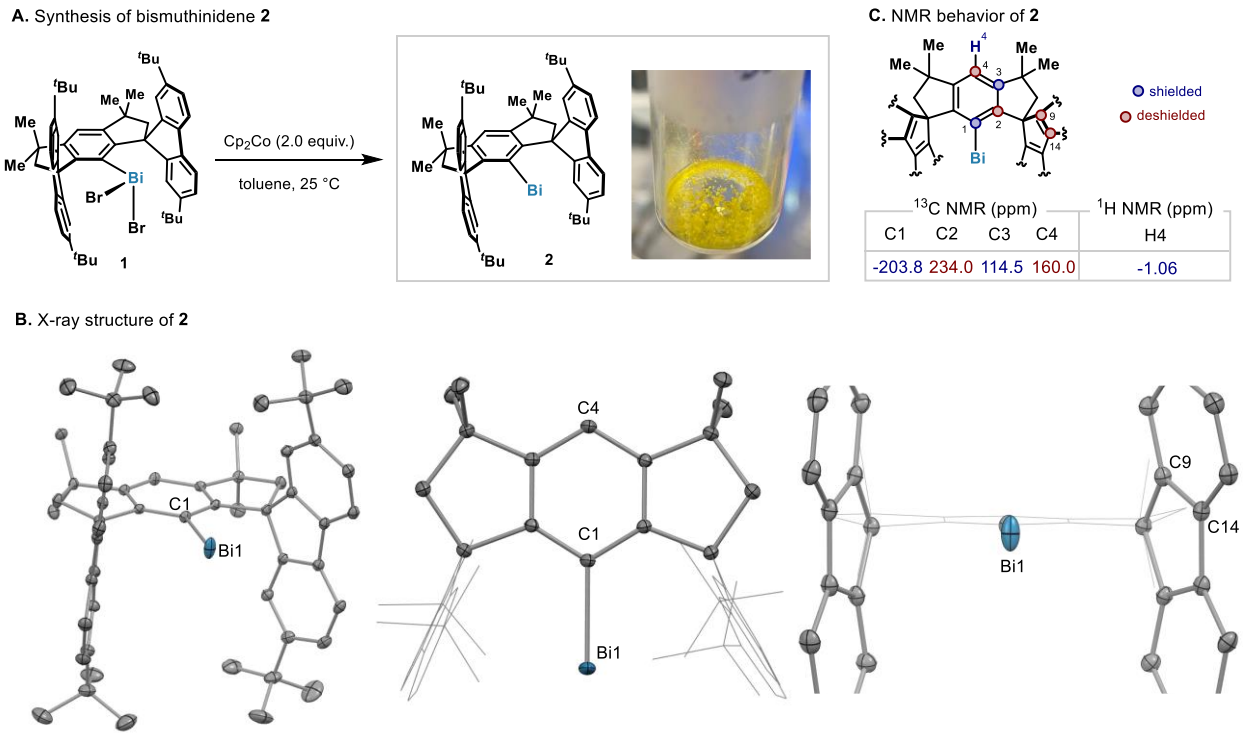

Fig. 2. A. Synthesis of the mono-coordinate bismuthinidene **2**. B. Solid state structure of **2** at 100K in different orientations. (thermal ellipsoids are displayed at a probability of 50% and H atoms were omitted for clarity). C. Unusual shielding-deshielding behavior of the aromatic C and H centers close to Bi in the ^{13}C and ^{1}H NMR (compared to **1** and **S3**).

Although most of the signals of **2** appear in the expected region of the NMR spectrum for diamagnetic compounds, anomalous shifts in certain ^{1}H and ^{13}C signals were clearly observed (Fig. 2C). Among these, H4 and C1 experience the most significant influences, shifting to remarkably shielded positions, from 7.69 and 208.9 ppm in the parent Bi(III) **1**, to −1.06 and −203.8 ppm in **2**, respectively. In previous reports, several unprecedented upfield ^{13}C NMR shifts were observed for those nuclei attached to paramagnetic transition metal centers (*34*, *35*). Interestingly, the chemical shifts of the atoms in the central phenyl ring of **2** display an alternating pattern: C1, C3 and H4 are shielded (−203.8, 114.5 and −1.06 ppm, respectively), whereas C2 and C4 are deshielded (234.0 and 160.0 ppm, respectively) (*36*). In spatial proximity to Bi, C9, C14

and their corresponding symmetry-related counterparts are also largely deshielded (177.7 and 176.9 ppm). Unlike common paramagnetic compounds (*16*), all NMR signals of **2** are sharp (except C1 due to quadrupole relaxation effects of ^{209}Bi, I = 9/2) and nearly temperature-independent. The chemical shifts of H-4 and C1 only change by 0.20 and 2.8 ppm, respectively, over a temperature range of 160 and 100 °C (see Supplementary Materials). Although **2** is highly air-sensitive, it exhibits remarkable stability in solution and solid state: The solid sample of **2** can be stored at ambient temperature under argon for months, and no noticeable decomposition was observed when a toluene-d_8 solution of **2** was heated up to 100 °C for 24 h.

The UV-vis-NIR spectrum of **2** shows no intense absorption in the visible region. Two weak bands are located at visible region (λ_{max} = 490 nm, $\varepsilon \approx 150$ M^{-1} cm^{-1}) and NIR region (λ_{max} = 1011 nm, $\varepsilon \approx 120$ M^{-1} cm^{-1}), indicating low energetic, spin-forbidden electronic transitions (Fig. S10 and Fig. 5B). A strong and unstructured fluorescence was observed with a maximum at 500 nm. Paramagnetic susceptibility was not detected for a powder sample of **2** in the temperature range of 1.8-300 K by using a SQUID magnetometer (Fig. 3A). This suggests that only the M_S = 0 magnetic sublevel has any appreciable Boltzmann population up to room temperature; this unprecedented experimental observation will be elaborated further in the theory section (*vide infra*).

Bi L_1-edge XAS data of **2** and a reference complex [Bi(III)Ph_3] are shown in Figure 3B (See SI for XAS measurements details), together with the corresponding TD-DFT calculated spectra. Based on the TD-DFT results, the absorption edge peak of **2** is dominated by the two lowest energy features corresponding to the electric dipole allowed 2s to 6p transitions. The peak position (16390.1 eV) in the XAS of **2** is noticeably lower than that of the Bi(III)Ph_3 (16392.3 eV), suggesting that the Bi atom is in the +1 oxidation state in **2**. Due to the large natural width of the 2s core level of Bi (12.4 eV) (*37*), the Bi L_1-edge XAS features are significantly broadened, which is in line with the FWHM of the absorption edge peak obtained in the XAS peak fitting (approx. 15 eV), making it unfeasible to deconvolute the experimental XAS spectra based on theoretical transitions. Nevertheless, the general experimental trends in Bi L_1-edge peak positions of known Bi(I)/Bi(III) reference complexes are reasonably reproduced by theory, and more importantly the experimental XAS data of **2** fit well with the theoretical Bi(I) model. It is also worth mentioning that the edge peak position of **2** (16390.1 eV) is not only lower than that of the Bi(III) atom in $BiPh_3$, but also lower than that of other known Bi(I) complexes, indicating the very unique electronic structure of the valence 6p orbitals of **2**. However, the 2s to 6p transition energies determined by TD-DFT calculations of the triplet, closed shell and open shell singlet models of **2** are nearly identical and are not possible to distinguish given the limited experimental resolution.

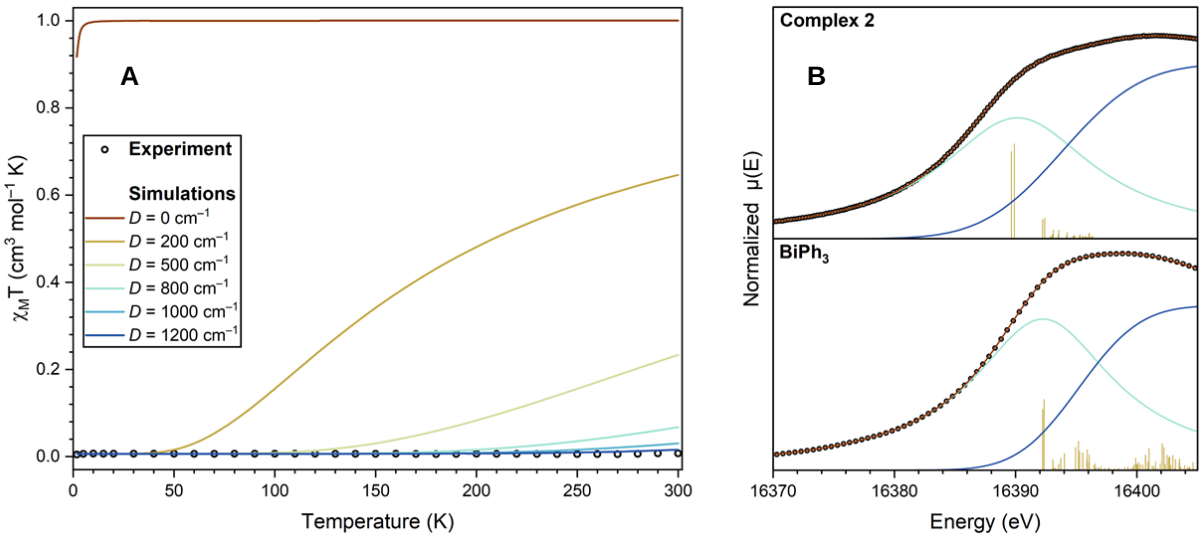

Fig. 3. Susceptibility and XAS measurements of **2**. A. Susceptibility: Temperature dependence of the molar magnetic susceptibility, $\chi_M T$ of **2**, measured with a powder sample and B = 1 T applied field. The experimental data are corrected for a diamagnetic contribution $\chi_{dia} = -633.2 \cdot 10^{-6}$ cm^3 mol^{-1}. The simulations accounted for only the z-direction of the susceptibility, χ_z, because the contributions of the x- and y-directions of the susceptibility are negligible in this system. The solid lines represent spin Hamiltonian simulations for a spin $S = 1$ with $g = 2$ and different values of the axial zero-field splitting parameter (D); B. XAS: experimental Bi L_1-edge XAS spectra with peak fitting results and TD-DFT calculated transitions of **2** (top) and $BiPh_3$ reference (bottom). For each sample, the absorption edge is modeled using a pseudo Voigt peak (cyan curve) and an error function background (blue curve) to fit (dark red curve) the experimental XAS spectra (black circles) between 16370 eV and 16405 eV (See SI for peak fitting details). The TD-DFT calculated absorption transitions (plotted as yellow vertical stick spectra) are shifted by a constant value of +312.4 eV based on the calibration established by XAS of the Bi(I)/Bi(III) reference complexes and their corresponding TD-DFT calculated energies (See Supplementary Materials for energy calibration details).

Additional experimental evidence of the +1 oxidation state at the Bi center of **2** is revealed by its reactivity patterns. Complex **2** reacts with methyl iodide and *N*-methyl maleimide, affording the corresponding oxidative addition complex **3** and the cycloaddition adduct **4**, respectively (Fig. 4). Whereas the former reaction is irreversible and **3** is isolated in high yield, the latter results in a temperature-dependent equilibrium between **2** and **4** (see Supplementary Materials).

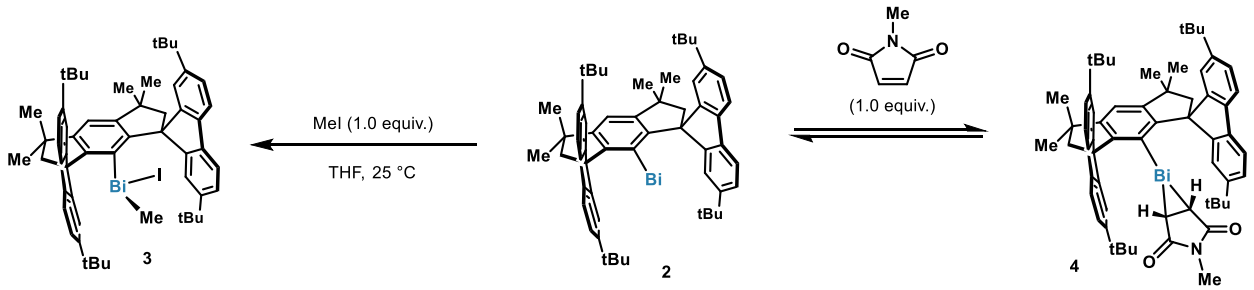

Fig. 4. Reactivity studies of complex **2**.

Insights into the intriguing experimental findings were obtained using quantum chemical calculations using the ORCA program package (*38*, *39*). We reasoned that for Bi(I), the Bi 6p-shell may contain two electrons in a triplet-, closed-shell singlet or open-shell singlet configuration. Consequently, initial geometry optimizations were performed using density functional theory (DFT) as described in the Supplementary Materials. Three sets of structures were optimized assuming a closed-shell singlet ground state, a triplet ground state and a broken-symmetry (BS) open-shell singlet electronic ground state. The triplet and BS geometries turned out to be exceedingly similar and distinctly different from the optimized closed-shell structure. The triplet/BS structures are in good to excellent agreement with experiment, while the closed-shell structure shows very large deviations from the X-ray crystal structure (see Supplementary Materials). From an energetic point of view, DFT predicts the Gibbs free energy of the triplet state to be lowest with the BS and closed-shell singlets calculated about 5 kcal/mol and 9 kcal/mol higher in energy, respectively. The reason for the triplet state being favored by the calculations is readily apparent by examining the singly occupied molecular orbitals (SOMOs) of the triplet state: they represent the in-plane and out-of-plane *p*-orbitals of the central Bi (Fig. 5A). These are almost pure Bi *p*-orbitals with little (<5%) admixture of the orbitals of the supporting ligands. However, the analysis of our theoretical results in terms of the atoms-in-molecules analysis indicates the presence of bond critical points that connect the bismuth center to the fluorenyl groups. In addition, there is the expected bond-critical point from the single bond between the bismuth and the C(sp2) of the aryl group.

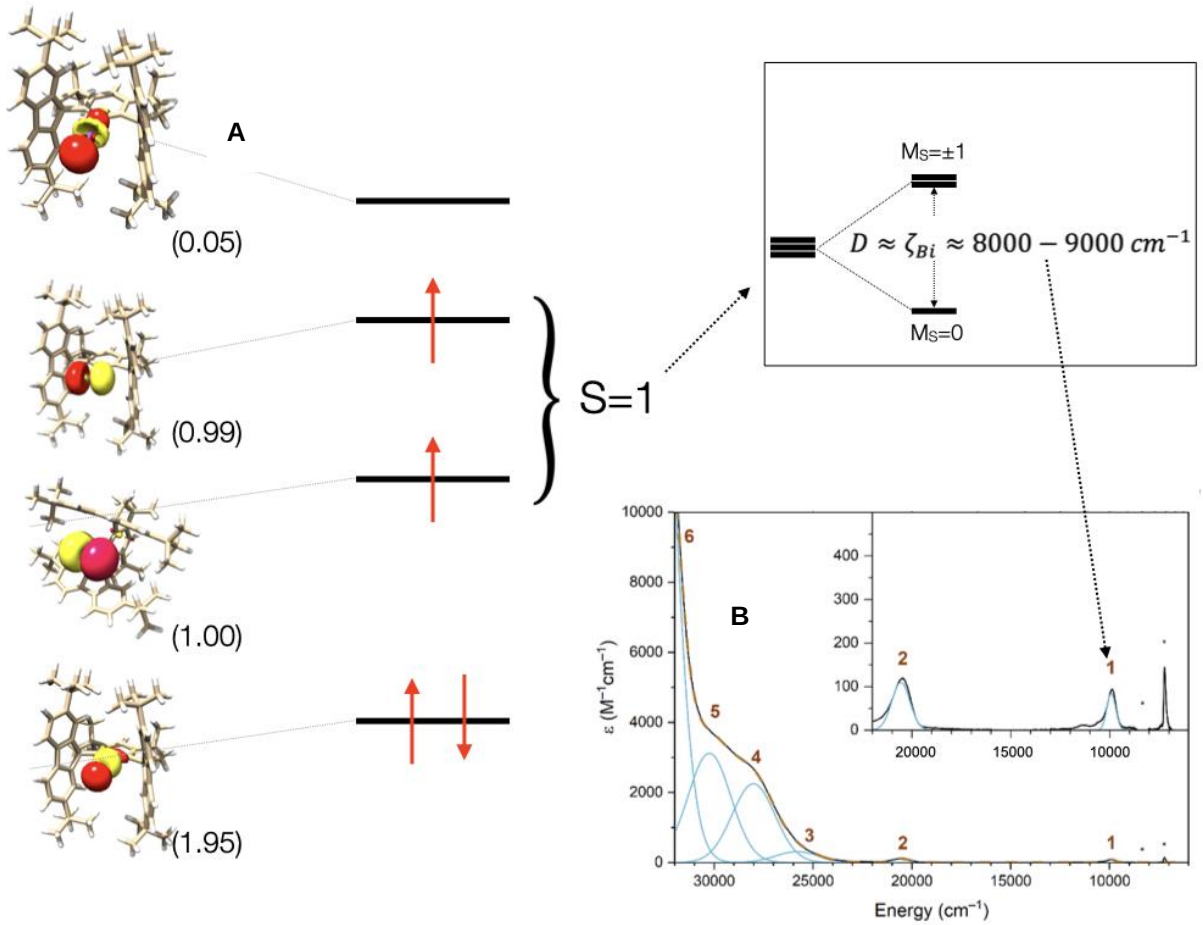

Fig. 5: A. Electronic structure of **2**. The central Bi(I) features four electrons in the 6p shell. In the electronic ground state, one electron pair forms a Bi–C bond with the ligand scaffold while two nearly degenerate lone-pairs are singly occupied with parallel spin electrons (natural orbital occupation numbers of a state specific CASSCF calculation are displayed in parenthesis). The three magnetic sublevels of the triplet ground state are split by the very large bismuth spin-orbit coupling interaction leading to a thermally isolated M_S=0 level lowest in energy. B UV-vis-NIR (0.352 mM of 2 in THF) resolved into individual Gaussian absorption bands labeled 1 to 6 and shown in blue. The arrows indicate our assigment of the UV-vis spectrum in terms of transitions from the lowest magnetic sublevel of the triplet ground state to the singlet configurations indicated by the level scheme above each absorption band. Solvent artifacts are labeled by asterisks in the experimental spectrum.

Taken at face value, these findings are fascinating: quantum chemistry leads to the sensible prediction that the ground state of **2** should be a triplet state while the magnetic measurements clearly demonstrate that **2** behaves diamagnetically. This seemingly stark contradiction can be resolved by proceeding to a more detailed treatment of the electronic structure offered by multi-configurational *ab initio* methods. Hence, complete active space self-consistent field (CASSCF) calculations were carried out at the DFT optimized geometries and dynamic electron correlation was incorporated using the N-electron valence second-order perturbation theory (NEVPT2). Initially, a minimal active space with two electrons in two-orbitals was pursued. The results of these calculations are in broad agreement with the DFT results in that they lead to a triplet ground state with the closed- and open-shell singlet states being higher in energy by about 10-15 kcal/mol. The results of state-averaged CASSCF and NEVPT2 calculations are very similar suggesting that the effects of dynamic electron correlation are limited for the determination of the ground state electronic configuration. Subsequently, the active space was extended to include all Bi 6*p*-orbitals

as well as the main σ-bonding orbital between the Bi atom and the ligand scaffold leading to a CAS(4,5) description. In these calculations, the scalar relativistic states (6 singlet and 5 triplets were determined to cover the spectrum up to about 50,000 cm^{-1} based on preliminary calculations) were allowed to interact via the spin-orbit coupling interaction (SOC). The results provide a striking explanation for the experimental findings. The ground state is still mainly composed of the spin-triplet state but contains a large (~24%) admixture of a closed- and open-shell singlet state. Importantly, the splitting in the magnetic sublevels (the M_S = 0, +1 and –1 components of the triplet state with S = 1) induced by the SOC are so large that a single magnetic sublevel remains thermally isolated; the $M_S = \pm 1$ components of the triplet state are of nearly 100% triplet character and are found about 4500 cm^{-1} higher in energy (Fig. 5A). In other words, complex **2** features an extremely large and positive axial zero-field splitting (ZFS) interaction that splits the M_S = 0 magnetic sublevel away from the $M_S = \pm 1$ states by more than 4500 cm^{-1}, which is equivalent to about 0.55 eV or >15 kcal/mol. Since this splitting is so large, the $M_S = \pm 1$ magnetic sublevels can never achieve any Boltzmann population in the susceptibility measurement up to room temperature. Moreover, there exists no possible transition that could be triggered by a microwave photon in the EPR experiments. Thus, one may refer to **2** as featuring a "non-magnetic triplet ground state". Based on the results of the NEVPT2 calculations, the band 1 found in the near IR region of the UV-vis spectrum of **2** around 10000 cm^{-1} (Fig. 5B) belongs to transitions from the Ms=0 magnetic sublevel of the ground state to the $M_S = \pm 1$ states. The calculated energies at 9940 and 10011 cm^{-1} are in excellent agreement with experiment. The weak band 2 (Fig. 5B) is assigned to triplet-singlet transition that becomes allowed by the strong scrambling between singlet and triplet states. It is calculated at 20596 cm^{-1}, again in excellent agreement with the experiment. The excited state corresponds to the configuration 2020 (singlet manifold double excitation).

In conclusion, we report the synthesis and isolation of a stable genuine bismuthinidene (**2**) featuring a single C(sp^2)–Bi bond and a fascinating electronic structure. The low-coordination number of the Bi center leaves two electrons in two nearly degenerate *p*-orbitals, thus resulting in a triple ground state. In addition, the intrinsically large SOC constant of Bi dramatically stabilizes the M_S=0 sublevel, leading to an apparent diamagnet. These properties combined result in a unique electronic situation for a main group compound, opening up new unchartered territories.

References and Notes:

1. R. A. Moss, M. S. Platz, M. Jones Jr., Eds., *Reactive Intermediate Chemistry* (Wiley, 2004).
2. J. Stöhr, H. C. Siegmann, Eds., *Magnetism: From Fundamentals to Nanoscale Dynamics* (Springer, 2006).
3. E. König, G. König, Eds., *Magnetic Properties of Coordination and Organometallic Transition-Metal Compounds* (Springer, 1981).
4. M. Gomberg, *Ber. Dtsch. Chem. Ges.* **33**, 3150–3163 (1900).
5. M. Gomberg, *J. Am. Chem. Soc.* **22**, 757–771 (1900).
6. P. P. Power, *Chem. Rev.* **103**, 789−809 (2003).
7. R. G. Hicks, Ed., *Stable Radicals: Fundamentals and Applied Aspects of Odd-Electron Compounds* (Wiley, 2010).

8. M. Abe, *Chem. Rev.* **113**, 7011−7088 (2013).
9. K. Hirai, T. Itoh, H. Tomioka, *Chem. Rev.* **109**, 3275–3332 (2009).
10. C. Wentrup, *Angew. Chem. Int. Ed.* **57**, 11508–11521 (2018).
11. L. Dostál, *Coord. Chem. Rev.* **353**, 142–158 (2017).
12. H. Tomioka, E. Iwamoto, H. Itakura, K. Hirai, *Nature* **412**, 626–628 (2001).
13. E. Iwamoto, K. Hirai, H. Tomioka, *J. Am. Chem. Soc.* **125**, 14664–14665 (2003).
14. F. Dielmann, *et al. Science* **337**, 1526–1528 (2012).
15. L. Liu, D. A. Ruiz, D. Munz, G. Bertrand, *Chem* **1**, 147–153 (2016).
16. J. Sun, *et al. Nat. Chem.* **12**, 1054–1059 (2020).
17. H. W. Moon, J. Cornella, *ACS Catal.* **12**, 1382−1393 (2022).
18. A. Heimer, E. Hulthén, *Nature* **127**, 557 (1931).
19. G. Herzberg, *Molecular Spectra and Molecular Structure, I. Spectra of Diatomic Molecules* (Van Nostrand, 1950).
20. D. P. Mukhopadhyay, *et al. Chem. Sci.* **11**, 7562−7568 (2020).
21. N. Tokitoh, Y. Arai, R. Okazaki, S. Nagase, *Science* **277**, 78−80 (1997).
22. B. Twamley, C. D. Sofield, M. M. Olmstead, P. P. Power, *J. Am. Chem. Soc.* **121**, 3357−3367 (1999).
23. H. J. Breunig, R. Rösler, E. Lork, *Angew. Chem. Int. Ed.* **37**, 3175−3177 (1998).
24. P. Šimon, F. de Proft, R. Jambor, A. Růžička, L. Dostál, *Angew. Chem. Int. Ed.* **49**, 5468−5471 (2010).
25. G. Wang, *et al. Chem. Eur. J.* **25**, 4335–4339 (2019).
26. M. M. Siddiqui, *et al. J. Am. Chem. Soc.* **143**, 1301–1306 (2021).
27. T. Matsuo, *et al. Bull. Chem. Soc. Jpn.* **84**, 1178–1191 (2011).
28. M. Mantina, *et al. J. Phys. Chem. A* **113**, 5806–5812 (2009).
29. P. Pyykkö, M. Atsumi, *Chem. Eur. J.* **15**, 186–197 (2009).
30. I. Vránová, *et al. Chem. Eur. J.* **21**, 16917–16928 (2015).
31. Y. Pang, M. Leutzsch, N. Nöthling, J. Cornella, *J. Am. Chem. Soc.* **142**, 19473–19479 (2020).
32. Y. Pang, M. Leutzsch, N. Nöthling, F. Katzenburg, J. Cornella, *J. Am. Chem. Soc.* **143**, 12487–12493 (2021).
33. J. D. Queen, A. Lehmann, J. C. Fettinger, H. M. Tuononen, P. P. Power *J. Am. Chem. Soc.* **142**, 20554-20559 (2020).
34. H. Fujii, *J. Am. Chem. Soc.* **124**, 5936–5937 (2002).
35. Y. Hiraoka, *et al. Dalton. Trans.* **44**, 13439–13443 (2015).
36. J. Vícha, *et al. Chem. Rev.* **120**, 7065–7103 (2020).
37. M. O. Krause, J. H. Oliver, *J. Phys. Chem. Ref. Data* **8**, 329-338 (1979).
38. F. Neese, F. Wennmohs, U. Becker, C. Riplinger, *J. Chem. Phys.* **152**, 224108 (2020).
39 F. Neese, Software update: The ORCA program system—Version 5.0. *WIREs Comput Mol Sci*. 12:e1606 (2022).
40. M. Wu, H. Li, W. Chen, D. Wang, Y. He, L. Xu, S. Ye, G. Tan, Chem 10.1016/j.chempr.2023.05.005

Supplementary References

41. R. Evans *et al. Angew. Chem., Int. Ed.* **52**, 3199-3202 (2013).
42. R. Evans, G. Dal Poggetto, M. Nilsson, G. A. Morris, *Anal. Chem.* **90**, 3987-3994 (2018).
43. Y. He, C. Dai, D. Wang, J. Zhu, G. Tan, *J. Am. Chem. Soc.* **144**, 5126-5135 (2022).
44. E. Welter, R. Chernikov, M. Herrmann, R. Nemausat, *AIP Conference Proceedings* **2054**, 040002 (2019).
45. S. Diaz-Moreno *et al. Journal of Physics: Conference Series* **190**, 012038 (2009).
46. S. Hayama *et al. Journal of Synchrotron Radiation* **25**, 1556-1564 (2018).
47. M. Newville, *Journal of Physics: Conference Series* **430**, 012007 (2013).
48. M. Newville, T. Stensitzki, D. B. Allen, A. Ingargiola, LMFIT: Non-Linear Least-Square Minimization and Curve-Fitting for Python. *Zenodo*, (2014).
49. E. van Lenthe, J. G. Snijders, E. J. Baerends, *J. Chem. Phys.* **105**, 6505-6516 (1996).
50. C. van Wüllen, *J. Chem. Phys.* **109**, 392-399 (1998).
51. A. D. Becke, *J. Chem. Phys.* **98**, 1372-1377 (1993).
52. P. J. Stephens, F. J. Devlin, C. F. Chabalowski, M. J. Frisch. J. Phys. Chem. 98, 11623–11627 (1994).
53. F. Weigend, R. Ahlrichs, *Phys. Chem. Chem. Phys.* **7**, 3297-3305 (2005).
54. D. A. Pantazis, F. Neese, *Theor. Chem. Acc.* **131**, 1292 (2012).
55. S. Grimme, J. Antony, S. Ehrlich, H. Krieg, *J. Chem. Phys.* **132**, 154104 (2010).
56. D. Bykov *et al. Mol. Phys.* **113**, 1961-1977 (2015).
57. C. Angeli, R. Cimiraglia, S. Evangelisti, T. Leininger, J. P. Malrieu, *J. Chem. Phys.* **114**, 10252-10264 (2001).

58. W. Kutzelnigg, W. Liu, *J. Chem. Phys.* **123**, 241102 (2005).
59. P. Pollak, F. Weigend, *J. Chem. Theory Comput.* **13**, 3696-3705 (2017).
60. Y. J. Franzke, R. Treß, T. M. Pazdera, F. Weigend, *Phys. Chem. Chem. Phys.* **21**, 16658-16664 (2019).
61. B. A. Heß, C. M. Marian, U. Wahlgren, O. Gropen, *Chem. Phys. Lett.* **251**, 365-371 (1996).
62. F. Neese, *J. Chem. Phys.* **122**, 034107 (2005).
63. F. Neese, E. I. Solomon *Inor. Chem.* **37**, 6568-6582 (1998).
64. D. Ganyushin, F. Neese *J. Chem. Phys.* **125**, 24103 (2006).
65. F. Neese, T. Petrenko, D. Ganyushin, G. Olbrich *Coord. Chem. Rev.* **251**, 288-327 (2007).
66. M. Atanasov, D. Ganyushin, K. Sivalingam, F. Neese "A modern first-principles view on ligand field theory through the eyes of correlated multireference wavefunctions" in *Molecular Electronic Structures of Transition Metal Complexes II*, vol. 142 of Sturcture and Bonding series, D. M. P. Mingos, P. Day, J. P. Dahl, Eds. (Springer, 2012), pp. 149-220.
67. M. Atanasov, D. Aravena, E. Suturina, E. Bill, D. Maganas, F. Neese *Coord. Chem. Rev.* **289-290**, 177-214 (2015).

Acknowledgements

We acknowledge DESY (Hamburg, Germany), a member of the Helmholtz Association HGF, for the provision of experimental facilities. Parts of this research were carried out at PETRA III under proposal I-20220137, and we would like to thank Dr. Edmund Welter for assistance in using P65 beamline. We acknowledge Diamond Light Source (UK) for experiment time on Beamline I20-scanning under proposal SP30449. We would like to thank Dr. Fred Mosselmans, Dr. Shu Hayama and Dr. Matteo Aramini for their assistance during the beamtime. We thank Prof. Dr. A. Fürstner for generous support. We also thank the analytical departments at the MPI Kohlenforschung for support (MS, NMR, Xray). **Funding**: Financial support for this work was provided by Max-Planck-Gesellschaft, Max-Planck-Institut für Kohlenforschung, Max Planck Institute for Chemical Energy Conversion, China Scholarship Council and Förderprogramm des Instituts Stipendium-Gästeprogramm (PhD Fellowships to Y.P.) and Fonds der Chemischen Industrie (FCI-VCI), European Union's Horizon 2020 research and innovation programme under Agreement No. 850496 (ERC Starting Grant, J.C.). **Author contributions**: Y.P. synthesized and isolated compounds **1**, **2**, **3**, **S1**, **S2** and **S3**. N.N. and R.G. determined the X-ray crystal structures. NMR analysis was conducted by M.L. and Y.P. EPR experiments were conducted by E.J.R. L.W. helped synthesizing the ligand. M.v.G. aided in the acquisition and interpretation of the UV-vis. E.B. and D.S. acquired and analyzed susceptibility data obtained via SQUID magnetometry. L.K. and S.D. acquired and analyzed XAS data. F.N. conducted theoretical calculations on the electronic structure of the complex. The manuscript was written by J.C., F.N. and Y.P. The project was directed by J.C. and F.N. **Competing interests**: The authors declare no competing financial interests. **Data and Materials**: Crystallographic data for structures **1**, **2**, **3**, **S1**, **S2** and **S3** are available free of charge from the Cambridge Crystallographic Data Center under reference numbers 2225004, 2225002, 2225006, 2225003, 2225005 and 2225007, respectively.

Supplementary Materials:

Materials and Methods

Supplementary text

Figs. S1 to S54

Tables S1 to S16

References (*40-61*)